NANO LETTERS

2004
Vol. 4, No. 10
1809−1814

Microarrays of Biomimetic Cells Formed by the Controlled Synthesis of Carbon Nanofiber Membranes

Benjamin L. Fletcher,[†] Eric D. Hullander,[†] Anatoli V. Melechko,[†] Timothy E. McKnight,[‡,§] Kate L. Klein,[†] Dale K. Hensley,[‡] Jennifer L. Morrell,[||] Michael L. Simpson,[†,‡,§] and Mitchel J. Doktycz*[,‡,||]

University of Tennessee, Knoxville, Tennessee 37996, Condensed Matter Sciences Division, Engineering Science and Technology Division and Life Sciences Division, Oak Ridge National Laboratory, P.O. Box 2008, MS 6123, Oak Ridge, Tennessee 37831

Received April 29, 2004; Revised Manuscript Received August 23, 2004

ABSTRACT

Biological processes are carried out in a small physical volume, the cell, where molecular composition coupled with defined nanometer-scale architecture bring about function. A major challenge inherent in copying this engineering ideal is the fabrication and filling of enclosed membrane structures. Described here is the combination of deterministically grown carbon nanofibers, micromachining techniques, and piezo-based ink jet technology to create cellular mimics. The synthesis, testing, and application of coupled arrays of semipermeable microstructures with defined, sub-nanoliter fluid contents are demonstrated.

Natural systems are recognized for their efficiency and functional diversity. They are capable of handling numerous inputs simultaneously, processing energy from their environment and transporting materials as needed. The elemental unit of these seemingly diverse systems is the cell, where complex biomolecular systems enable function. The physical aspects of the cell are especially important for enabling its diverse roles. The small size of biological cells, and their component sub-structures, enables intra- and intercellular molecular processing by simple, diffusion-based transport mechanisms. Even large macromolecules can diffuse across micron-scale distances very rapidly, reducing the need for further organization. When required, natural systems employ nanoscale architectures to further facilitate network function. Well-known examples include cellular organelles, co-localized enzymes that enable metabolic processing,[1] and various architectural networks used for transporting materials and for performing mechanical functions.[2−4] Further, within the small fluid volume of a cell, small changes in molecular numbers result in significant changes in concentration, leading to altered reaction conditions and concentration gradients that drive the transport of information through genetic and biochemical circuits and networks.

Imitating the multiple length scale detail of the cell presents an opportunity to exploit Nature's engineering principles. To realize this ideal requires the controlled synthesis of nanoscale features within structures that are microns and millimeters in size. Such dimensions are within the range of typical nanomaterials and micromachining techniques. Guided by biological example, the combination of these structures and technologies can greatly impact technological devices. However, significant challenges face the synthesis of biologically related nanostructures. One limitation to building cellular mimics is the construction and filling of cells separated by semipermeable membranes. A fluid, lipid bilayer membrane envelops natural cells and serves as both a container and a controller of the chemical reactions inside the cell. Cellular reagents are exchanged with the neighboring environment by the use of precisely engineered pore structures. Transport through a membrane is diffusion controlled but can be extremely rapid due to the nanometer scale dimensions of the membrane. For mimicking biological cells, the incorporation of semipermeable barriers, or membranes, is a necessity. These membranes must be able to selectively control the transport of molecular species, requiring engineering on the nanometer scale.

Unfortunately, the use of natural membrane components, lipid bilayers, can lead to fragile structures and systems that are difficult to precisely engineer with present technology. Further, techniques for creating arrays of adjoined structures

* Corresponding author. E-mail: doktyczmj@ornl.gov.
[†] University of Tennessee.
[‡] Condensed Matter Sciences Division, ORNL.
[§] Engineering Science and Technology Division, ORNL.
[||] Life Sciences Division, ORNL.

10.1021/nl0493702 CCC: $27.50
Published on Web 09/09/2004

are not readily apparent. A variety of synthetic membrane structures, based on either micromachining or nanoengineering techniques[5−14] have been described. Typically, these structures, and material flow, are perpendicular to the plane of the substrate. This can lead to long pore lengths, increasing diffusion-based transport rates. If thin support structures are used, the material can become fragile. Another approach to creating sieving structures is to create obstacles that are perpendicular to the plane of the substrate for impeding flow parallel to the surface. For example, post structures have been used as synthetic gel media in the electrophoretic separation of biomolecules.[15,16] In this approach to sieving, the distance between the outer edges of the obstacles defines the "pore". The use of nanoscale post structures offers the possibility of even finer control of the separation criteria and reduced transport distances. Such structures can be fabricated from vertically aligned carbon nanofibers.[17] These structures can be deterministically grown, allowing for control over the length, diameter, shape, position, orientation, and chemical composition of the nanofiber.[18−23] Further, carbon nanofibers offer a modifiable surface and can be combined with microfluidic,[17] electronic,[24−27] and biological structures.[28] The physical and functional characteristics of carbon nanofibers allow for the design of robust membrane structures that enable rapid, diffusion-based transport and integration with other synthetic devices.

To demonstrate the fabrication of cellular mimics, microscale arrays of carbon nanofibers were patterned within microfluidic structures. Photolithography and reactive ion etching (RIE) were used first to pattern microfluidic structures onto a silicon wafer. Shipley 1813 photoresist was spun on a 100 mm diameter silicon wafer at 4000 rpm for 1 min and baked at 115 °C for 1 min. Then, the channels were exposed through a contact mask and the photoresist was developed in Shipley CD-26. The residual resist was removed by RIE in an O_2-based plasma for 30 s. This left the channels bare, and the rest of the wafer coated in photoresist (Figure 1A). Then, inductively coupled (ICP) SF_6-based plasma RIE was used to etch the channels out of the silicon. The channels were etched at varying depths, 8, 10, 12, and 15 μm (Figure 1B). Without removing the photoresist from the previous step, another layer of Shipley 1813 photoresist was spun on the wafer at 4000 rpm for 1 min and baked at 115 °C for 1 min. Preserving the photoresist from the previous step is crucial for eliminating artifacts that are created by spinning photoresist over nonplanar structures. Then using contact lithography, the photoresist was exposed to create a grid pattern in the bottom of the microfluidic channel. An image reversal was then performed by baking in NH_3 atmosphere at 90 °C. This was followed by 2 min of flood exposure, 5 min of development in CD-26, and 30 s of RIE in O_2 plasma (Figure 1C). The Ti (100 Å) wetting layer and Ni (400 Å) catalyst layer were then deposited by electron beam evaporation. The wafer was then soaked in acetone, lifting off the sacrificial photoresist and leaving only the lines of catalyst that define the cell membranes (Figure 1D). The thickness of the cell membrane was set at 2 μm by defining the width of the nickel catalyst stripe. The vertically aligned carbon

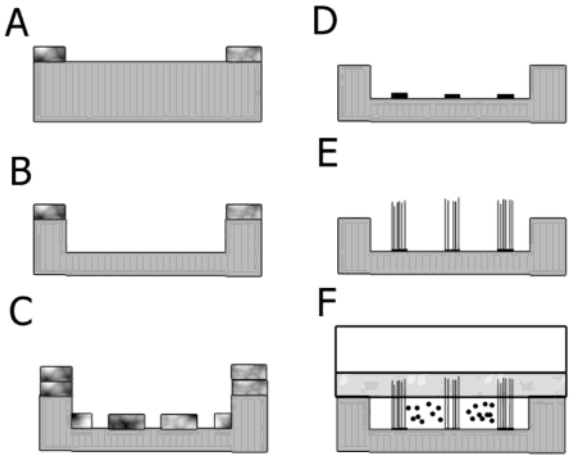

Figure 1. Diagram of the microfabrication process viewed in cross section. (A) The channel pattern is defined in photoresist. (B) The microfluidic channels are etched into the Si substrate. (C) The grid pattern, for producing cells, is defined in the second layer of photoresist. (D) Catalyst metal (Ni) is deposited. (E) VACNFs are grown by PECVD. (F) Cross section of final structure, sealed with a PDMS layer that is supported by a glass slide.

nanofibers were grown using a plasma enhanced chemical vapor deposition process in a C_2H_2/NH_3 dc plasma (100 mA, 3 Torr, 55 sccm of C_2H_2, 80 sccm NH_3) (Figure 1E). Annealing and etching of the Ni film prior to growth breaks the contiguous film into nanoparticles with an average spacing and size that depends on the film thickness, thereby defining the pore size in the membrane. Individual fibers grow from each Ni nanoparticle as a result of the catalytic decomposition of acetylene and the diffusion of carbon through the nickel particle, subsequently depositing carbon layers in a vertical fashion. Thinner membrane structures or defined spacing of the carbon nanofibers can be prescribed by electron beam lithography or by control of the catalyst layer.[29] For these studies, a catalyst layer of 40 nm was used. This led to nanofiber densities of 1 to 4 nanofibers/μm^2. This correlates to interfiber spacings on the order of 250 to 500 nm. Individual nanofibers are slightly conical in shape, with the nanofiber height and aspect ratio being controlled by the growth conditions.[20] For cell mimic construction, the fibers were grown at least ~8 μm taller than the channel depth to ensure sealing of the structure (Figure 1F, discussed below). Electron micrographs of the cell mimic structures are shown in Figure 2.

Reagents are deposited into individual cells using a piezo-based reagent jetting system (MicroFab Technologies, Inc., Plano, TX) mounted onto a custom video microscope. Piezo-based reagent delivery dispenses extremely small volumes and is compatible with biomolecule patterning.[30] For these studies, size specific, fluorescently labeled latex beads (Polysciences, Inc., Warrington, PA) were used to evaluate the carbon nanofiber membranes. Dispensed volumes depend on the nozzle diameter (30 μm) of the piezo jet and were on the order of 15 pL. The resulting droplet is easily contained within the cell; however, water droplets on this scale evaporate within minutes and complicate assembly. Drying can harm biological reagents and also causes the latex beads to become fixed to the silicon surface. Therefore, to

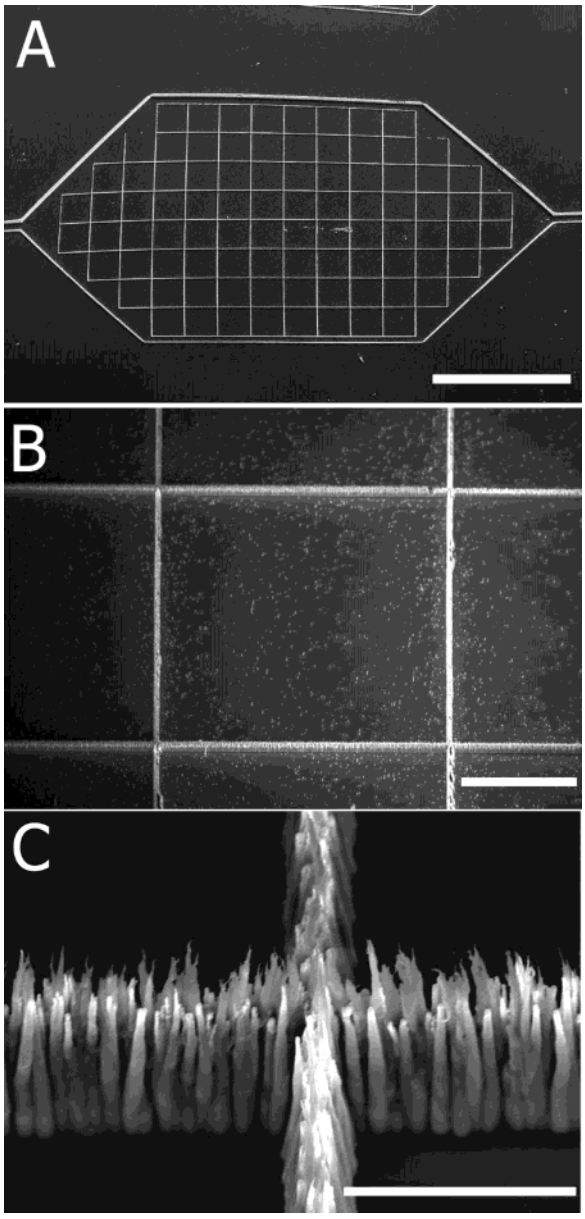

Figure 2. Electron micrographs of the cell mimic structure. Panel A illustrates the overall design of the cell mimic device and the integrated microfluidic structure. The microfluidic inlet and outlet channels that allow fluid flow to the array of the cell structures are 50 μm wide and 10 μm deep. Panels B and C (30° viewing angle) show close-ups of a single cell and the component nanofibers, respectively. The scale bars are 1 mm, 100 μm, and 10 μm on A, B, and C, respectively.

facilitate fabrication and testing, beads were dispersed in a 25% aqueous glycerol solution. The addition of glycerol reduces evaporation rates, enabling unhurried processing between dispensing and sealing of the structures. The use of DMSO was also found suitable, but led to spreading of the droplet upon dispensing. Glycerol solutions greater than 25% have the further advantage of preventing the latex particles from falling out of suspension. Latex beads as large as 750 nm remained suspended even after centrifugation of 1% bead solutions in 25% glycerol for five minutes at 9300× g (data not shown). Although latex beads remained suspended, the beads can still adhere strongly to the silicon surface, preventing subsequent dispersion. The addition of phosphate buffered saline to the dispensing solution partially alleviated this problem. Blocking of the silicon surface with (1%) bovine serum albumin further reduced the adhesion to acceptable levels.

Several approaches to sealing the cell mimic structures are possible but they must be limited to those that preserve the integrity of the dispensed reagents. Therefore adhesives, high temperatures, low pressures, and solvents were avoided. These requirements create an unusual challenge as they prohibit the use of many standard and proven sealing techniques.[31] Matching the fiber height and the etch depth can enable the use of hard materials as a lid structure; however it was found that minor differences in nanofiber height can prevent effective sealing of the membranes to the upper surface. Sealing with a soft polymer such as poly(dimethylsiloxane) (PDMS) is advantageous as the nanofibers can be grown to extend beyond the channel depth and pierce the lid structure to create a floor-to-ceiling barrier. However, upon sealing, the soft polymer can also sag and adhere to the silicon surface in the cell interior. This interferes with the dispensed droplet and complicates subsequent wetting of the structure. These problems were remedied by supporting a thin layer of PDMS with a glass slide. PDMS coatings were approximately 4 μm thick and prepared by coating a glass slide with a viscous PDMS solution, placing the slide on edge and allowing for gravity to thin the coating. Upon curing, the PDMS-coated glass slide was then clamped onto the cell mimic structure using ordinary paper binder clips (small, 9.5 mm capacity). Upon sealing, an enclosed fluidic structure is created with individual cell volumes on the order of 250 pL.

The efficacy of the device was evaluated by dispensing 750-nm diameter fluorescently labeled latex beads into selected cells. Figure 3 displays fluorescent micrographs of the cell mimic structure before and after sealing and wetting of the device. Before sealing, the fluorescent spots indicate the dispense locations (Figure 3A). After sealing, the structures are wetted by flowing buffer solution (100 mM Tris, pH 8.0) through the microfluidic channel using either capillary action or application of vacuum at the downstream terminus. The wetting solution was of similar constitution as the dispensed droplets and can be easily exchanged by aspiration of the fluid through the microchannel. As can be seen in Figure 3B, the latex beads are dispersed but contained within individual cell structures. The beads remain contained even after fluidic exchange. Individual beads can be observed to diffuse within individual cells and occasionally are also found to aggregate or adhere to the cell surfaces (Figure 3B). Wetted structures show similar characteristics even after several weeks of storage and multiple exchanges of fluid. Further evidence of effective sealing is confirmed by post-experiment evaluation of the lid structure. Electron micrographs show that the nanofiber membranes pierce the PDMS lid and are sometimes retained in the PDMS (data not shown).

The size dependent containment limits of the carbon nanofiber membrane structures were evaluated using a range

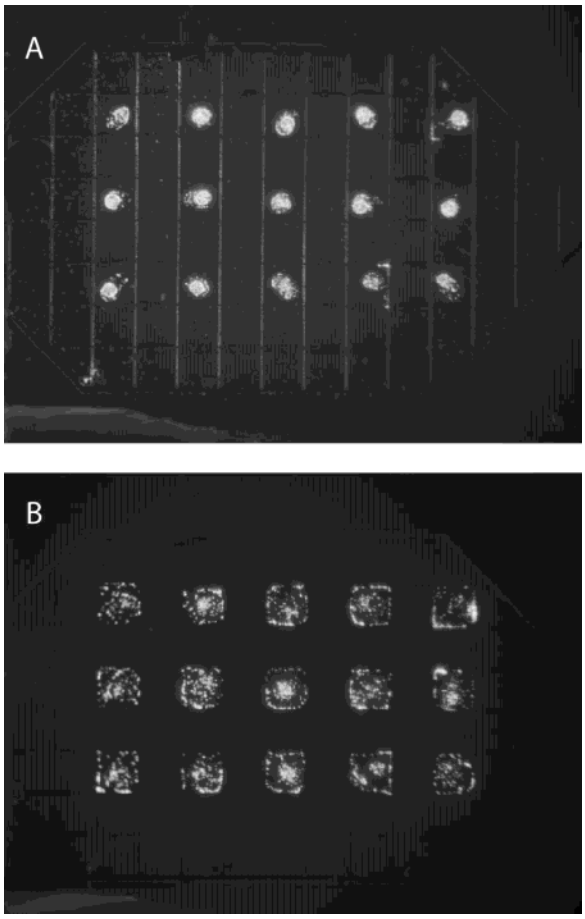

Figure 3. Filling and sealing of cell mimic structures. (A) Individual cells within the array are filled by dispensing a 0.02% solution of 750 nm diameter fluorescein-labeled latex beads from a piezoelectric reagent jet. The location of the dispensed droplets is seen in the fluorescent micrograph at top. (B) The bottom panel shows the same area after sealing and wetting of the structure.

of latex bead sizes. Images of cell mimic structures that were filled with latex beads of a particular size, varying from 300 to 500 nm in diameter, are displayed in Figure 4. Complete containment is observed for bead diameters that are greater than 500 nm. This is consistent with measurements of the nanofiber density and diameter. Partial containment is observed for beads as small as 100 nm (the smallest size tested) as nanofibers are often packed within a spacing of only a few tens of nanometers. However, on average, the spacing is much higher. For experiments involving the smaller sized beads, leaking is often observed at distinct locations within the membrane structure. The stochastic placement of carbon nanofibers within the defined membrane areas prevents precise definition of the membrane pore size and leaking at specific sites.

Currently, the membrane pore size is too large to contain macromolecules such as proteins, but several approaches can be considered to further constrict the free space between the nanofibers. Electron beam lithography can be used to define the site of catalyst placement.[20] This would enable membrane fabrication with predefined thickness and nanofiber spacing. Single rows of carbon nanofibers should be possible, enabling extremely short transport distances without compromising

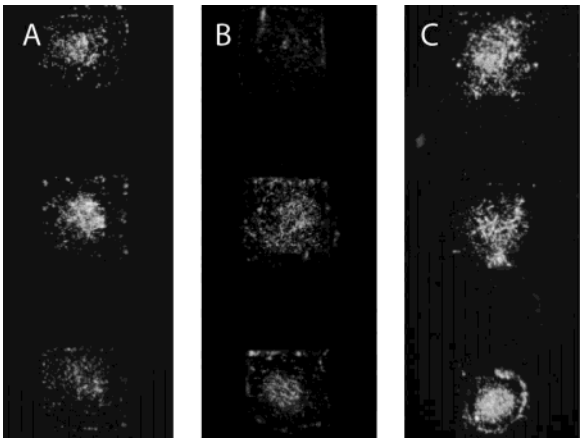

Figure 4. Membrane containment limits of cell mimic structures. Shown are fluorescent micrographs of a portion of a cell mimic structure that was filled with (A) 500 nm, (B) 400 nm, or (C) 300 nm fluorescein-labeled latex beads. Complete containment is observed for 500 nm beads, but leaking is observed for beads smaller than 400 nm.

the physical strength of the membrane. Interfiber spacings down to 10 or 20 nm may be possible with nanoscale lithographies. Another approach to reducing the free space between nanofibers is to coat the structures with other materials. Previous work has shown that carbon nanofibers are compatible with resist coatings,[32,33] oxide deposition,[34] and metal deposition by either electrochemical or evaporative means.[36] Specific addressing of nanofibers through chemical, electrochemical,[12] or lithographic means can enable modification of either specific nanofibers or regions of nanofibers within the membrane. This could enable definition of the direction and type of transport through the membrane leading to further mimicry of biological cell membranes.

The reagent jet dispensing technique allows for specific addressing of individual cells within the matrix of neighboring cells. This enables patterning and integration of fluid phase reagents with the multiple length scale physical structures created by the combination of nanoscale and microscale fabrication techniques. This integration is essential for mimicking biological cells and for creating more complex structures. To demonstrate the ability to specifically address individual cells, latex beads containing either red or green fluorescent labels were dispensed into specific cells within the matrix (Figure 5). To accomplish this, the reagent jetting system deposited one type of bead, then was washed and refilled with the second reagent. Simultaneous, parallel dispensing should be possible with multiple reagent jets for more rapid construction. As seen in Figure 5, different reagents can be contained within specific cells, while fluid diffuses throughout the entire structure. This arrangement can allow for the transport of soluble reagents throughout the device while other soluble reagents remain spatially constrained, analogous to multicellular structures where transferable reagents enable cell-to-cell communication. This feature can also be exploited for array-based analyses, as commonly employed for biological screening.[37] Typically, microarray-based assays rely on patterning and immobilizing probe molecules on a substrate surface. Surface immobiliza-

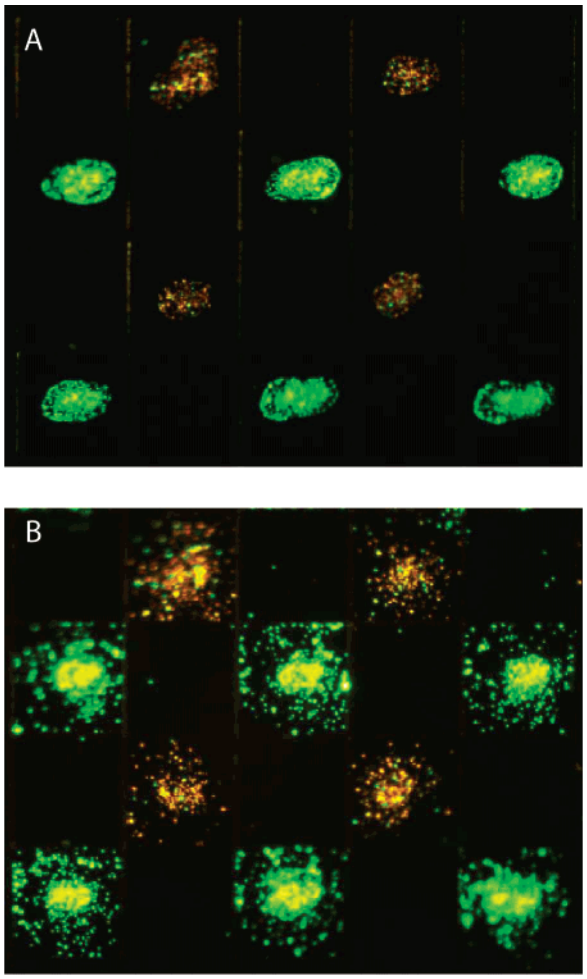

Figure 5. Addressing of individual cells within a matrix of cellular mimics. Shown is a portion of a cell mimic structure that was selectively filled with either 500 nm fluorescein-labeled latex beads or 500 nm tetramethylrhodamine-labeled latex beads in selected cells. (A) Fluorescence micrograph showing the location of the dispensed droplets before sealing of the structure. (B) The same area after sealing and wetting of the structure. The different reagents stay contained in their respective cells.

tion can cause denaturation of macromolecular structure, loss of biological activity, hindered access to reactive sites, and slow reaction kinetics. Arrayed fluid phase reagents can overcome many of these shortcomings by allowing the probe molecules to diffuse freely in solution. Further, the three-dimensional cell volume allows for careful control of the reagent concentration and increased binding capacity.

To demonstrate the use of arrayed cells with fluidic connectivity, *E. coli* were dispensed into individual cells of the cell mimic matrix (Figure 6A). The bacterial cells were dispensed in a solution of 25% glycerol and Luria broth to prevent dehydration and promote growth. The bacterial cells contain a plasmid that encodes for a green fluorescent protein (GFP) to assist in visualization. Upon sealing and wetting of the structure with growth media, the bacterial cells divide yet stayed contained within the cell mimic structure (Figure 6B). Examination through a microscope shows that a large fraction of the bacteria are mobile, while other bacteria appear to settle on the surface. Typical *E. coli* cells are rod shaped ($\sim 3 \times 1\ \mu$m). These dimensions are larger than the

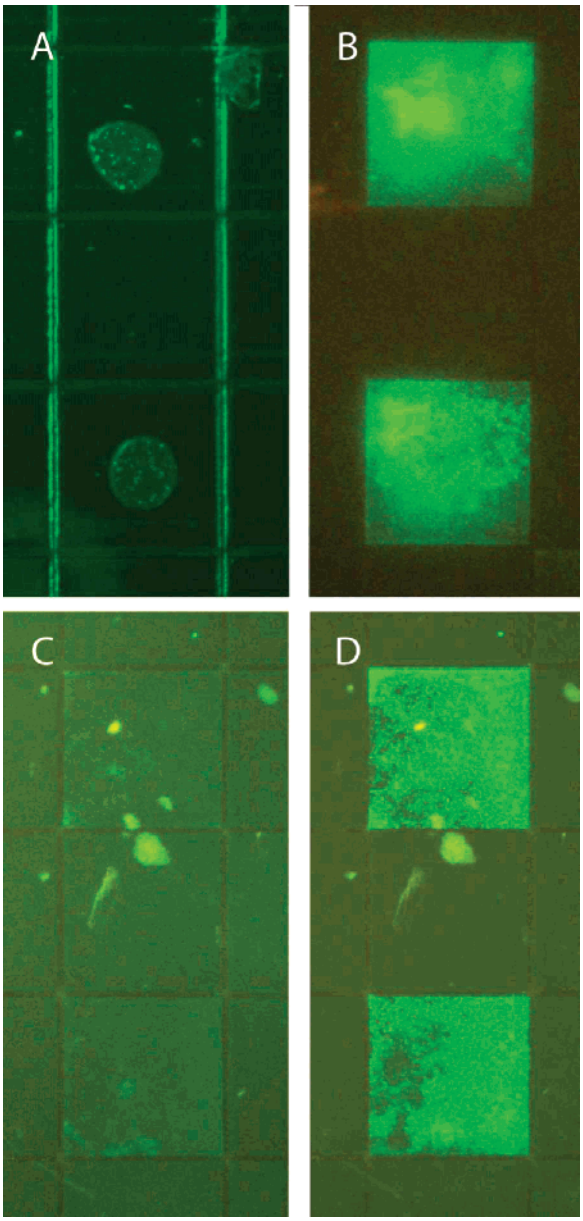

Figure 6. Caging of *E. coli* within the cell mimic structure. Bacteria were deposited into individual cells of the cell mimic structure (A) and grown in the presence of growth media (B). In (A) and (B), *E. coli* strain BL21(DE3) (Invitrogen, Carlsbad, CA), constitutively expressing GFP from a plasmid, was used. In (C) and (D), *E. coli* strain BL21(DE3) expressing a GFP-DivIVA-GroEL2 fusion protein under control of the pBAD promoter was dispensed into alternating cells in the cellular mimic structure. The structure was immersed in LB medium with 50 μg/mL ampicillin to maintain selection of the plasmid and left to incubate at 37 °C for 12 h. Following this incubation, expression of the GFP fusion protein was induced by adding 0.2% arabinose to the medium and flowing it through the structure. These images show three adjacent cells in the structure, with bacteria present in the upper and lower cells. (C) before induction and (D) 3 h after arabinose induction.

measured interfiber spacing, and thus the bacteria stay contained in the cell mimic structure.

The "caging" of bacteria can be useful for studies on chemical signaling and for construction of live cell based sensing systems. Figures 6C and D display an example of this latter application. *E. coli* cells containing a plasmid

expressing a GFP fusion protein under the control of an inducible promoter were deposited into the cell mimic structure. The promoter controls gene expression and is sensitive to the presence of arabinose. After overnight growth of the bacteria in the absence of arabinose, fluorescence is not detectable due to the lack of gene expression (Figure 6C). However, upon flowing arabinose containing media through the microfluidic channel, expression of the GFP fusion promoter is induced in the cells, enabling visualization of the bacteria. Such a system could be useful for evaluating the effects of the chemical and physical environment on gene expression by arraying bacteria that contain GFP under the control of different promoters. Alternatively, the utility of whole-cell approaches for specific sensing of chemical reagents[38] can be expanded by allowing the deployment of multiple distinct bioreporter strains on the same chip.

The cell mimic structures could be further miniaturized for creating higher density devices. Further miniaturization would augment functionality by facilitating diffusion-based transport. Such a transport mechanism would nicely complement and interface to microfluidics-style pumping mechanisms. Integration with other microscale structures, such as electronic systems, would make possible communication between man-made devices and solution-based reaction systems. Copying the scale of biological systems will lead to an effective interface to them. New approaches to disease treatment, "smart" sensors, dosing devices, tissue scaffolds and even surrogate tissues could be realized. Most significantly, a cell mimic platform provides an appropriate tool for evaluating biochemical reactions where physical conditions more closely match those of a natural cell. This allows for copying the functionality of natural systems at a fundamental level, enabling a universal platform capable of great utility. Cellular attributes including multiple sensing capabilities, signal amplification, logic processing, chemical release, mechanical actuation, and energy transformation would be realized by employing the complex reaction systems inherent in biochemical networks. Integration with further nanopatterning could allow for "sub-cellular" organization and further mimicry. The use of a cellular structure in Nature is universal. The variations and functions of naturally occurring cells indicate that the application of its engineering principles may be limitless.

Acknowledgment. We thank Rob Ilic (Cornell) for assistance with mask making and Pam Fleming for metal depositions. This research was supported by NIH Grant EB000657 and the Material Sciences and Engineering Division Program of the DOE Office of Science. This work was performed at the Oak Ridge National Laboratory, managed by UT-Battelle, LLC, for the U.S. DOE under Contract No. DE-AC05-00OR22725.

References

(1) Hochachka, P. W. *Proc. Natl. Acad. Sci. U.S.A.* **1999**, *96*, 12233.
(2) Pratt, W. B.; Silverstein, A. M.; Galigniana, M. D. *Cell Signal* **1999** *11*, 839.
(3) Volkmann D.; Baluska F. *Microsc. Res. Tech.* **1999**, *47*, 135.
(4) Ellis, R. J. *Trends Biochem. Sci.* **2001**, *26*, 597.
(5) Fendler, J. H. *Advances in Polymer Science*; Springer-Verlag: Berlin, 1994.
(6) Pearson, D. H.; Tonucci, R. J. *Science* **1995**, *270*, 68.
(7) Park, M.; Harrison, C.; Chaikin, P. M.; Register, R. A.; Adamson, D. H. *Science* **1997**, *276*, 1401.
(8) Desai, T. A.; Chu, W. H.; Tu, J. K.; Beattie, G. M.; Hayek, A.; Ferrari, M. *Biotech. Bioeng.* **1998**, *57*, 118.
(9) Martin, C. R.; Nishizawa, M.; Jirage, K.; Kang, M.; Lee, S. B. *Adv. Mater.* **2001**, *13*, 1351.
(10) Li, J.; Stein, D.; McMullan, C.; Branton, D.; Aziz, M. J.; Golovchenko, J. A. *Nature* **2001**, *412*, 166.
(11) Cao, H.; Yu, Z.; Wang, J.; Tegenfeldt, J. O.; Austin, R. H.; Chen, E.; Wu, W.; Chou, S. Y. *Appl. Phys. Lett.* **2002**, *81*, 174.
(12) Tzu-Chi Kuo, T.-C.; Cannon, D. M., Jr.; Chen, Y.; Tulock, J. J.; Shannon, M. A.; Sweedler, J. V.; Bohn, P. W. *Anal. Chem.* **2003**, *75*, 1861.
(13) Melechko, A. V.; McKnight, T. E.; Guillorn, M. A.; Merkulov, V. I.; Ilic, B.; Doktycz, M. J.; Lowndes, D. H.; Simpson, M. L. *Appl. Phys. Lett.* **2003**, *82*, 976.
(14) Hinds, B. J.; Chopra, N.; Rantell, T.; Andrews, R.; Gavalas, V.; Bachas, L. G. *Science* **2004**, *303*, 62.
(15) Volkmuth, W. D.; Austin, R. H. *Nature* **1992**, *358*, 600.
(16) Turner, S. W.; Perez, A. M.; Lopez, A.; Craighead, H. G. *J. Vac. Sci. Technol. B* **1998**, *16*, 3835.
(17) Zhang, L.; Melechko, A. V.; Merkulov, V. I.; Guillorn, M. A.; Simpson, M. L.; Lowndes, D. H.; Doktycz, M. J. *Appl. Phys. Lett.* **2002**, *81*, 135.
(18) Melechko, A. V.; Merkulov, V. I.; Lowndes, D. H.; Guillorn, M. A.; Simpson, M. L. *Chem. Phys. Lett.* **2002**, *356*, 527.
(19) Merkulov, V.; Melechko, A. V.; Guillorn, M. A.; Lowndes, D. H.; Simpson, M. L. *Chem. Phys. Lett.* **2002**, *361*, 492.
(20) Merkulov, V. I.; Hensley, D. K.; Melechko, A. V.; Guillorn, M. A.; Lowndes, D. H.; Simpson, M. L. *J. Phys. Chem. B* **2002**, *106*, 10570.
(21) Merkulov, V. I.; Melechko, A. V.; Guillorn, M. A.; Lowndes, D. H.; Simpson, M. L. *Appl. Phys. Lett.* **2002**, *80*, 476.
(22) Merkulov, V. I.; Melechko, A. V.; Guillorn, M. A.; Lowndes, D. H.; Simpson, M. L. *Chem. Phys. Lett.* **2001**, *350*, 381.
(23) Merkulov, V. I.; Melechko, A. V.; Guillorn, M. A.; Simpson, M. L.; Lowndes, D. H.; Whealton, J. H.; Raridon, R. J. *Appl. Phys. Lett.* **2002**, *80*, 4816.
(24) Guillorn, M. A.; McKnight, T. E.; Melechko, A.; Merkulov, V. I.; Britt, P. F.; Austin, D. W.; Lowndes, D. H.; Simpson, M. L. *J. Appl. Phys.* **2002**, *91*, 3824.
(25) Guillorn, M. A.; Melechko, A. V.; Merkulov, V. I.; Hensley, D. K.; Simpson, M. L.; Lowndes, D. H. *Appl. Phys. Lett.* **2002** *81*, 3660.
(26) Li, J.; Cassell, A.; Delzeit, L.; Han, J.; Meyyappan, M. *J. Phys. Chem. B* **2002**, *106*, 9299.
(27) Li, J.; Ng, H. T.; Cassell, A.; Fan, W.; Chen, H.; Ye, Q.; Koehne, J.; Han J.; Meyyappan M. *Nano Lett.* **2003**, *3*, 597.
(28) McKnight, T. E.; Melechko, A. V.; Griffin, G. D.; Guillorn, M. A.; Merkulov, V. I.; Serna, F.; Hensley, D. K.; Doktycz, M. J.; Lowndes, D. H.; Simpson, M. L. *Nanotechnology* **2003**, *14*, 551.
(29) Merkulov, V. I.; Lowndes, D. H.; Wei, Y. Y.; Eres, G.; Voelkl, E. *Appl. Phys. Lett.* **2000**, *76*, 3555.
(30) Calvert, P. *Chem. Mater.* **2001**, *13*, 3299.
(31) Duffy, D. C.; McDonald, J. C.; Schueller, O. J. A.; Whitesides, G. M. *Anal. Chem.* **1998**, *70*, 4974.
(32) Guillorn, M. A.; Melechko, A. V.; Merkulov, V. I.; Ellis, E. D.; Simpson, M. L.; Baylor L. R.; Bordonaro, G. J. *J. Vac. Sci. Technol. B* **2001**, *19*, 2598.
(33) McKnight, T. E.; Melechko, A. V.; Guillorn, M. A.; Merkulov, V. I.; Doktycz, M. J.; Culbertson, C. T.; Jacobson, S. C.; Lowndes, D. H.; Simpson, M. L. *J. Phys. Chem. B* **2003**, *107*, 10722.
(34) Melechko, A. V.; McKnight, T. E.; Guillorn, M. A.; Austin, D. W.; Ilic, B.; Merkulov, V. I.; Doktycz, M. J.; Lowndes, D. H.; Simpson, M. L. *JVST B* **2002**, *20*, 2730.
(35) Guillorn, M. A.; McKnight, T. E.; Melechko, A.; Merkulov, V. I.; Britt, P. F.; Austin, D. W.; Lowndes, D. H.; Simpson, M. L. *J. Appl. Phys.* **2002**, *91*, 3824.
(36) Yang, X. J.; Guillorn, M. A.; Austin, D.; Melechko, A. V.; Cui, H. T.; Meyer, H. M.; Merkulov, V. I.; Caughman, J. B. O.; Lowndes, D. H.; Simpson, M. L. *Nano Lett.* **2003**, *3*, 1751.
(37) Heller, M. J. *Annu. Rev. Biomed. Eng.* **2002**, *4*, 129.
(38) Simpson, M. L.; Sayler, G. S.; Ripp, S.; Nivens, D. E.; Applegate, B. M.; Paulus, M. J.; Jellison, G. E., Jr. *Trends Biotechnol.* **1998**, *16*, 332.

NL0493702